The Astronomical Journal, 129:2643–2653, 2005 June

OLD GLOBULAR CLUSTERS MASQUERADING AS YOUNG IN NGC 4365?

Jean P. Brodie, Jay Strader, Glenda Denicoló, Michael A. Beasley, and A. J. Cenarro
UCO/Lick Observatory, University of California, Santa Cruz, CA 95064; brodie@ucolick.org, strader@ucolick.org, denicolo@tlaloc.inaoep.mx, mbeasley@ucolick.org, cen@astrax.fis.ucm.es

Søren S. Larsen and Harald Kuntschner
European Southern Observatory, Karl-Schwarzschild-Strasse 2, D-85748 Garching, Germany; slarsen@eso.org, hkuntsch@eso.org

and

Duncan A. Forbes
Centre for Astrophysics and Supercomputing, Swinburne University, Hawthorn, VIC 3122, Australia; dforbes@astro.swin.edu.au
Received 2004 November 5; accepted 2005 February 19

ABSTRACT

High signal-to-noise ratio, low-resolution spectra have been obtained for 22 globular clusters (GCs) in NGC 4365. Some of these were selected as probable representatives of an intermediate-age (2–5 Gyr), extremely metal-rich GC subpopulation. The presence of such a subpopulation had been inferred from the unusual optical and near-infrared color distributions of GCs in this otherwise typical Virgo elliptical galaxy. However, ages derived from Lick indices are consistent with uniformly old mean ages for all GCs in our sample. The metallicities of the clusters show some evidence of a *trimodal* distribution. The most metal-poor and metal-rich peaks are consistent with the values expected for an elliptical galaxy of this luminosity, but there appears to be an additional, intermediate-metallicity peak lying between them. New *Hubble Space Telescope* photometry is consistent with this result. A plausible scenario is that in earlier data these three peaks merged into a single broad distribution. Our results suggest that it is difficult to identify intermediate-age GC subpopulations solely with photometry, even when both optical and near-infrared colors are used.

Key words: galaxies: evolution — galaxies: individual (NGC 4365) — galaxies: stellar content — globular clusters: general

1. INTRODUCTION

Several studies have demonstrated that the color distributions of the globular cluster (GC) systems of luminous early-type galaxies are usually found to be bimodal—the color distribution is better represented by a superposition of two Gaussian functions than by a single Gaussian, typically with a high level of statistical significance (Ashman et al. 1994; Gebhardt & Kissler-Patig 1999; Kundu & Whitmore 2001; Larsen et al. 2001). The vast majority of these studies have been carried out in the V and I passbands, and the peaks of the Gaussians consistently occur at or around $V-I\sim0.95$ and 1.18. This almost ubiquitous bimodality indicates the common presence of subpopulations and suggests that multiple mechanisms and/or epochs of formation have been at work in producing the GC systems and, by implication, the parent galaxies themselves. Since there is an age-metallicity degeneracy in optical broadband colors, it is not possible to determine from optical photometry alone whether the color difference is due to an age or a metallicity difference between the subpopulations or some combination of the two. If both subpopulations are old, like those in the Milky Way (∼10–13 Gyr), the color difference would correspond to a metallicity difference of ∼1 dex in [Fe/H]. In general, a younger subpopulation appears bluer for a given metallicity.

The giant elliptical galaxy NGC 4365, located in the outskirts of the Virgo Cluster, has previously been noted as a puzzling possible exception to the bimodality rule. Its *Hubble Space Telescope* (*HST*) WFPC2 $V-I$ color distribution is unimodal and broad (Forbes 1996; Gebhardt & Kissler-Patig 1999; Larsen et al. 2001). Hundreds of GCs were detected in these studies, indicating that the unimodality cannot be attributed to small number statistics. Puzia et al. (2002) suggested, based on a combination of optical and near-infrared photometry, that a significant fraction of the GCs in NGC 4365 are of intermediate age (2–5 Gyr) and are extremely metal-rich (between solar and 3 times solar metallicity). Such intermediate-age clusters might fill in the gap between the blue and red peaks in a "normal" color distribution, causing it to appear unimodal and unusually wide for a single subpopulation. Using Keck spectroscopy, Larsen et al. (2003, hereafter Paper I) estimated ages and metallicities for a sample of 14 confirmed GCs and found evidence that some, although not all, of the candidate intermediate-age clusters were intermediate-age and metal-rich ($-0.4\lesssim$ [Fe/H] $\lesssim 0$). Interestingly, the derived metallicities were significantly lower than those determined by Puzia et al. on the basis of the extremely red $V-K$ colors of the clusters.

In the context of GCs as probes of the formation histories of galaxies, these results presented something of a contradiction. While early work suggested stellar population differences between the main body of the galaxy and its kinematically decoupled core (Surma & Bender 1995), a more recent study found a luminosity-weighted age of ∼14 Gyr and constant [Mg/Fe] for both components (Davies et al. 2001). NGC 4365 shows no evidence of a recent merger. If a significant subpopulation of intermediate-age GCs is indeed present in this galaxy, where are the intermediate-age galaxy stars that should accompany it? In Paper I we pointed out that at most 2%–3% of the mass of the galaxy could be in a stellar population with an age of 2–5 Gyr without strongly affecting its old integrated spectrum.

Here we revisit the NGC 4365 GC system with a new Keck spectroscopic study that yielded 22 confirmed GCs, three of

which are in common with Paper I. The new sample is of higher signal-to-noise ratio (S/N) than the previous work. Diagnostic absorption-line indices have been measured on these new spectra and compared with the most recent simple stellar population (SSP) models to derive ages and metallicities for the individual GCs. New *HST* Advanced Camera for Surveys (ACS) data for NGC 4365, obtained in the g and z bands, provide a better baseline for metallicity determinations than the WFPC2 $V-I$ data used in previous studies. The larger sample, superior data quality, and more sophisticated stellar evolutionary synthesis models allow a more reliable estimate of the distribution of ages and metallicities in the NGC 4365 GC system.

In § 2 we discuss the observations and data reduction techniques. In § 3 we derive radial velocities, ages, metallicities, and [α/Fe] ratios for the GCs in our sample. In § 4 we present the analysis of *HST* ACS g and z photometry for NGC 4365. Section 5 has discussion and conclusions.

2. OBSERVATIONS AND DATA REDUCTION

The spectra were obtained in multislit mode on 2003 March 23 and 24 using the Low Resolution Imaging Spectrometer (LRIS) (Oke et al. 1995) on the Keck I telescope. Candidate GCs were selected from V and I preimaging from FORS1 on the Very Large Telescope (VLT) UT1. Exposure times were 3×140 s in V and 3×190 s in I. The FORS photometry was roughly calibrated using *HST* WFPC2 data for NGC 4365 (Larsen et al. 2001; Kundu & Whitmore 2001). GC candidates were selected on the basis of luminosity and spatial distribution, covering a range of galactocentric radii out to $1.5r_e$ (Fig. 1). Both blue and red candidates were selected, and we specifically chose several of the possible intermediate-age GCs identified in Puzia et al. (2002). The sample included three objects from our previous study: our objects 6, 8, and 13 are objects 2, 5, and 11 in Paper I. During the observations, the slit mask was aligned at a position angle of 25°. Seventeen exposures, each with an integration time of 30 minutes, yielded a total exposure time of 510 minutes (8.5 hr) for each GC.

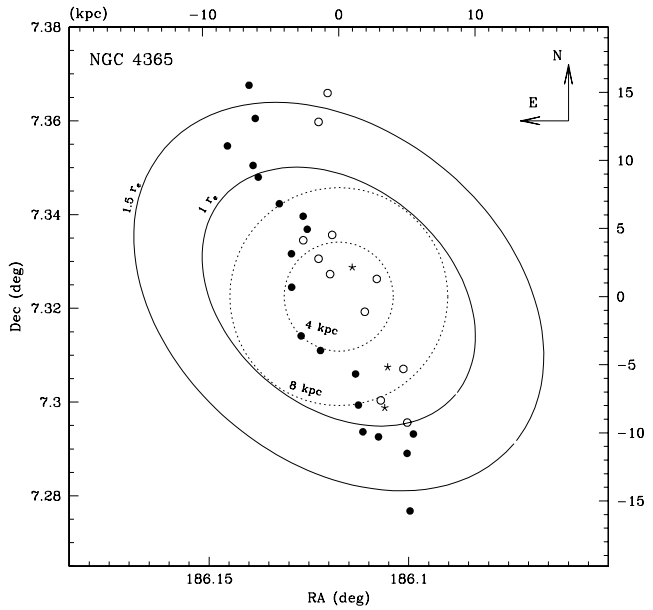

FIG. 1.—Spatial distribution for NGC 4365 GCs. The filled circles indicate GCs with spectra from this work; the open circles indicate those from Paper I. The stars indicate overlapping GCs from the two samples. The dotted circles represent radii of 4 and 8 kpc, while the solid ellipses represent the approximate isophotal contours of the stellar light at $1r_e$ and $1.5r_e$.

TABLE 1
GLOBULAR CLUSTER CANDIDATES IN NGC 4365

ID	R.A. (J2000.0)	Decl. (J2000.0)	V (mag)	$V_{\rm helio}$ (km s^{-1})	GC?
1.....	12 24 23.9	07 16 36	21.2	752 ± 14	GC
2.....	12 24 24.1	07 17 21	22.0	1732 ± 14	GC
3.....	12 24 23.7	07 17 36	21.7	635 ± 15	GC
4.....	12 24 25.8	07 17 33	21.9	1030 ± 14	GC
5.....	12 24 26.8	07 17 37	21.5	1226 ± 11	GC
6.....	12 24 25.4	07 17 56	22.3	1418 ± 14	GC
7.....	12 24 27.0	07 17 58	22.0	919 ± 12	GC
8.....	12 24 25.3	07 18 27	21.2	1592 ± 12	GC
9.....	12 24 27.2	07 18 22	21.0	1252 ± 13	GC
10.....	12 24 27.3	07 18 35	18.4	111 ± 16	Star
11.....	12 24 29.3	07 18 40	22.0	1326 ± 11	GC
12.....	12 24 30.5	07 18 51	20.7	1329 ± 9	GC
13.....	12 24 27.4	07 19 44	21.9	496 ± 14	GC
14.....	12 24 31.0	07 19 28	21.4	1563 ± 10	GC
15.....	12 24 31.0	07 19 54	21.7	1097 ± 10	GC
16.....	12 24 30.1	07 20 13	21.0	983 ± 15	GC
17.....	12 24 30.3	07 20 23	21.5	898 ± 14	GC
18.....	12 24 31.8	07 20 32	21.4	1206 ± 9	GC
19.....	12 24 33.0	07 20 53	21.5	1246 ± 13	GC
20.....	12 24 33.4	07 21 02	21.2	1501 ± 13	GC
21.....	12 24 34.9	07 21 17	22.5	986 ± 9	GC
22.....	12 24 33.2	07 21 38	22.3	985 ± 12	GC
23.....	12 24 33.6	07 22 03	22.0	980 ± 16	GC
24.....	12 24 35.1	07 22 16	22.3	22230 ± 34	Galaxy

NOTE.—Units of right ascension are hours, minutes, and seconds, and units of declination are degrees, arcminutes, and arcseconds.

The blue side of the LRIS, with a 600 line mm^{-1} grism, provided a wavelength coverage of ~3800–5600 Å. Flux standards G191-B2B, Hiltner 600, and PG 0934+554, as well as Lick/IDS standard stars from Worthey et al. (1994), were observed. The Lick standard stars were also used as radial velocity standards with kinematic information extracted from SIMBAD.[1] The slitlets in the mask employed on the first night were 0.″8 wide, matching the excellent seeing. The 1.″0 slit mask was chosen for the second night, during which the seeing varied between 1.″0 and 1.″2. Relevant properties for the cluster candidates are listed in Table 1. The V photometry is from our FORS imaging.

All the data reduction was carried out under IRAF.[2] The images were bias-subtracted and flat-field-corrected. Cosmic rays were carefully removed from each frame. After correction for optical distortions, each individual spectrum was extracted. Following wavelength calibration based on arc lamps mounted within the spectrograph, flux calibration was applied, and the individual spectra of each GC candidate were combined to optimize the S/N. After measuring the radial velocities (see below), small corrections to the wavelength calibration were made by cross-correlating the co-added spectra with appropriate spectral energy distributions from the new MILES stellar population models (A. Vazdekis et al. 2005, in preparation).

3. KINEMATICS, AGES, AND METALLICITIES

3.1. *Radial Velocities*

Radial velocities were determined by cross-correlating the target spectra with velocity standards. The radial velocities listed

[1] SIMBAD is operated at CDS, Strasbourg, France.

[2] IRAF is distributed by the National Optical Astronomy Observatory, which is operated by the Association of Universities for Research in Astronomy, Inc., under contract with the National Science Foundation.

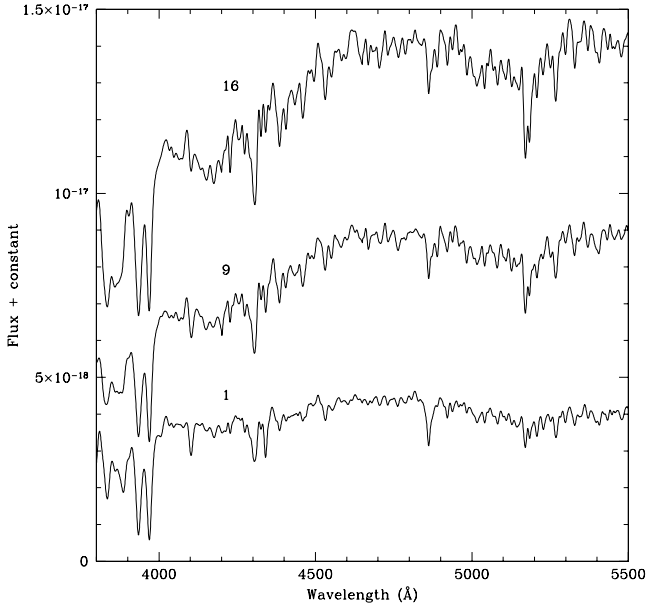

FIG. 2.—Spectra of GCs 1 (metal-poor), 9 (intermediate-metallicity), and 16 (metal-rich), smoothed to the Lick resolution. See text for details on the GC subpopulations.

in Table 1 are an average of the cross-correlation results for each reference star; the errors are estimates of the standard error of the mean based on six measurements. Of 24 candidate GCs, one object was found to be a foreground star, and a second object appears to be a $z \sim 0.07$ emission-line galaxy, leaving 22 confirmed GCs. These have a mean radial velocity of 1143 ± 67 km s^{-1} and a dispersion of 315 km s^{-1}, consistent with the value of 1227 ± 13 km s^{-1} from the Third Reference Catalogue of Bright Galaxies (de Vaucouleurs et al. 1991). The GC subpopulations (see below) do not show significant differences in their mean velocities or dispersions.

GC 4 shows Hβ fill-in and [O III] emission at 4959 and 5007 Å, suggesting that it contains a planetary nebula. We defer discussion of this cluster to a future paper and do not include it in our subsequent analysis. Smoothed spectra for three of our sample GCs are shown in Figure 2.

3.2. *Lick Indices and Ages*

Lick indices were measured using the definitions in Trager et al. (1998) and Worthey & Ottaviani (1997) after using a wavelength-dependent Gaussian kernel to smooth the final combined spectra to the Lick resolution. Errors were calculated statistically as the standard error of the mean of indices of the individual spectra of each GC candidate and checked by bootstrapping. The index measurements and associated errors are given in Tables 2 and 3. Measurements of Lick indices on six standard stars showed no significant deviations from the Lick system (although errors in offset determinations were large compared to the deviations themselves) and offsets generally smaller than the GC index errors. Thus, we did not apply them to our indices, but we have included them in Table 4 for completeness.

The Lick index values were compared with SSP model predictions to estimate ages and metallicities for the GCs. The models of Thomas et al. (2004, hereafter TMK04) were selected for this comparison. The TMK04 models are based on the "α-enhanced" models of Thomas et al. (2003, hereafter TMB03), but they incorporate the α-dependence of the higher order Balmer lines (Hγ and Hδ) in addition to the Hβ-dependence included in TMB03. These models are the only ones currently available that explicitly account for the α-enhancement known to dominate the abundance patterns in Milky Way GCs and thus expected to be present in extragalactic GCs.

Figures 3–5 show TMK04 SSP model grids for $[\alpha/\mathrm{Fe}] = +0.3$ along with Balmer line indices (Hβ, Hγ_F, and Hδ_F) versus [MgFe]$'$ for the 21 GCs in our new sample. [MgFe]$'$ (defined in TMB03 as $[\mathrm{Mg}b(0.72\ \mathrm{Fe5270} + 0.28\ \mathrm{Fe5335})]^{1/2}$) varies only weakly with $[\alpha/\mathrm{Fe}]$. Weighted means of the three subpopulations (see below) are overplotted. The distribution of points in Figures 3–5 is consistent with a uniformly old ($\sim$10–13 Gyr) GC population with a spread of metallicity from $[Z/\mathrm{H}] \sim -1.35$ to just above solar, although none appear to be far above solar. All three of the Balmer line indices present a largely consistent picture of old ages for all clusters, although individual cluster ages cannot be determined accurately. Ages derived from Hγ_F for the metal-rich GCs are slightly younger. Using the wider Hγ_A and Hδ_A index definitions instead of Hγ_F and Hδ_F gives consistent results.

A feature obvious in Figure 5 (and noticeable, although less clearly, in Figs. 3 and 4) is the grouping of objects into three distinct areas, suggesting the presence of *three* subpopulations of clusters. The weighted subpopulation means are consistent with this interpretation. All galaxies that have been spectroscopically studied to date have been found to contain at most two old subpopulations of GCs. Additional evidence of these three subpopulations, which we term metal-poor (blue), intermediate-metallicity (orange), and metal-rich (red), is explored more fully in § 4 using new *HST* ACS photometry.

For a more quantitative analysis of GC ages we used the χ^2 minimization technique of Proctor et al. (2004), which utilizes the entire suite of Lick indices to derive ages and metallicities for each GC. For most clusters all the indices through Fe5406 were used except CN_1 and CN_2. The resulting mean subpopulation ages are 11 ± 1 Gyr (blue), 11 ± 2 Gyr (orange), and 10 ± 1 Gyr (red). Systematic errors could affect these ages; thus, they should not be taken as absolute. However, they do illustrate that the three subpopulations are coeval within the errors.

In Figures 3–5 the location of the galaxy itself in the model grids is indicated by a star. Index values for the galaxy are taken from J. H. Howell (2005, in preparation) for all indices except Hδ_F, which is from Denicoló et al. (2005). These points represent an $r_e/8$ aperture at the galaxy center. The galaxy shows no detectable [O III]; thus, no emission correction was required. (However, Hα is not included in our spectra.) Since J. H. Howell (2005, in preparation) find $[\alpha/\mathrm{Fe}] = +0.26 \pm 0.04$ for NGC 4365, our use of $[\alpha/\mathrm{Fe}] = +0.3$ model grids is reasonable. The age of the galaxy is $\sim$7 and 4 Gyr derived from Hβ and Hγ_F, respectively, but $\sim$13 Gyr derived from Hδ_F. The 7 Gyr age we derive from Hβ is $\sim$5 Gyr younger than that reported by Davies et al. (2001), although our Hβ index measurements are quite similar. The difference in the age estimate is entirely due to model differences; Davies et al. used the models of Vazdekis (1999), while we use the models of TMK04. This discrepancy nicely illustrates the fact that SSP models do not offer reliable absolute age estimates. The relative rankings of galaxies and GCs in age and metallicity should be more robust, modulo such factors as horizontal-branch morphology, the luminosity function of the red and asymptotic giant branches, and the difficulty of model calibration at supersolar metallicities. These effects remain as uncertainties in SSP models (e.g., Schiavon et al. 2004; Maraston et al. 2001).

While the center of NGC 4365 does appear to be slightly younger than its GC system, it is important to remember that the

TABLE 2

LICK INDICES OF GLOBULAR CLUSTERS

ID	$H\delta_A$ (Å)	$H\delta_F$ (Å)	CN_1 (mag)	CN_2 (mag)	Ca4227 (Å)	G4300 (Å)	$H\gamma_A$ (Å)	$H\gamma_F$ (Å)	Fe4383 (Å)	Ca4455 (Å)	Fe4531 (Å)	Fe4668 (Å)	$H\beta$ (Å)	Fe5015 (Å)	Mg_1 (mag)	Mg_2 (mag)	Mg*b* (Å)	Fe5270 (Å)	Fe5335 (Å)	Fe5406 (Å)
1.....	1.47	1.80	0.003	0.031	0.29	3.10	−1.20	1.06	2.02	0.71	2.12	0.85	2.64	2.37	0.042	0.102	1.53	1.39	1.48	1.01
2.....	1.46	1.15	−0.012	0.015	0.66	3.49	−1.27	0.44	1.24	0.76	1.75	1.77	2.29	2.37	0.039	0.105	1.86	1.67	1.05	1.06
3.....	−0.08	0.32	0.037	0.048	0.47	3.89	−2.93	0.55	4.56	0.40	2.31	2.09	1.76	2.54	0.068	0.162	2.59	1.60	1.55	1.08
5.....	−1.94	−0.11	0.076	0.111	0.90	5.58	−5.16	−0.71	4.38	1.04	2.42	2.89	1.82	5.82	0.068	0.199	3.29	3.00	1.63	1.24
6.....	1.52	1.16	−0.053	−0.037	0.15	2.59	−0.13	1.29	1.90	0.22	1.44	0.02	2.56	2.97	0.030	0.101	1.54	1.43	0.46	0.38
7.....	1.49	1.38	−0.031	−0.008	0.44	3.66	−1.57	0.75	1.00	0.06	1.00	0.75	1.86	2.81	0.059	0.108	1.72	1.23	0.74	0.15
8.....	−0.13	0.95	0.048	0.087	1.11	4.44	−3.66	−0.20	3.62	0.80	2.86	2.82	1.88	4.46	0.071	0.190	3.29	2.03	1.39	1.38
9.....	−0.65	1.12	0.075	0.117	0.69	4.21	−3.34	−0.05	3.28	0.91	2.23	2.04	1.50	3.26	0.083	0.188	2.99	2.49	1.82	1.27
11.....	−0.86	−0.81	0.063	0.068	0.71	5.26	−3.95	0.40	4.08	1.31	3.44	3.31	2.15	6.81	0.076	0.206	3.15	2.45	1.00	0.39
12.....	−0.30	0.80	0.046	0.081	0.80	4.22	−3.24	0.02	3.15	1.06	3.08	2.48	2.23	3.95	0.051	0.172	3.10	1.87	1.65	1.28
13.....	−0.21	0.98	0.068	0.098	1.26	3.89	−3.15	0.10	2.53	1.41	3.11	5.37	1.08	5.22	0.087	0.214	3.47	2.10	1.49	1.35
14.....	−0.24	0.80	0.032	0.070	0.87	4.85	−3.62	−0.02	3.51	0.97	2.15	3.35	2.02	4.30	0.068	0.180	3.02	1.68	1.65	0.80
15.....	−0.61	0.73	0.066	0.100	0.92	4.32	−3.93	−0.57	3.46	0.83	3.27	3.62	1.67	5.28	0.082	0.226	3.78	2.74	1.61	1.33
16.....	−2.05	−0.08	0.136	0.177	1.06	5.07	−5.48	−1.24	4.80	1.32	3.35	4.24	1.45	4.82	0.107	0.258	4.41	2.78	2.11	1.66
17.....	0.10	0.88	0.061	0.106	0.45	3.91	−2.72	0.10	2.98	0.77	2.56	2.80	1.85	3.44	0.061	0.159	2.29	1.97	1.67	1.15
18.....	−1.39	0.57	0.106	0.143	0.68	4.54	−4.31	−0.48	4.01	1.05	2.67	3.29	2.00	4.84	0.090	0.219	3.69	2.59	1.86	1.35
19.....	−0.18	0.57	0.047	0.075	0.69	4.58	−4.17	−1.08	1.74	0.75	3.23	1.56	1.76	4.03	0.059	0.180	3.14	1.81	1.81	1.20
20.....	0.89	1.28	−0.016	0.011	0.66	4.16	−2.44	0.43	2.21	0.77	2.25	1.84	2.06	3.31	0.041	0.116	1.83	1.26	1.32	0.97
21.....	2.15	1.77	−0.003	0.027	0.68	4.03	−2.04	0.77	3.88	1.61	1.01	0.87	2.30	4.49	0.049	0.116	1.87	1.27	2.45	0.78
22.....	2.04	2.15	−0.005	0.032	0.22	3.42	−2.76	0.02	2.97	0.17	1.82	1.95	2.44	2.56	0.025	0.124	3.17	0.63	1.41	1.65
23.....	1.31	1.66	−0.016	0.025	0.25	3.14	0.04	1.62	0.98	0.50	1.74	1.19	1.71	3.04	0.031	0.104	2.03	1.26	1.69	0.48

TABLE 3

LICK INDEX ERRORS

ID	$H\delta_A$ (Å)	$H\delta_F$ (Å)	CN_1 (mag)	CN_2 (mag)	Ca4227 (Å)	G4300 (Å)	$H\gamma_A$ (Å)	$H\gamma_F$ (Å)	Fe4383 (Å)	Ca4455 (Å)	Fe4531 (Å)	Fe4668 (Å)	$H\beta$ (Å)	Fe5015 (Å)	Mg_1 (mag)	Mg_2 (mag)	Mg *b* (Å)	Fe5270 (Å)	Fe5335 (Å)	Fe5406 (Å)
1.....	0.35	0.19	0.008	0.008	0.17	0.31	0.27	0.16	0.40	0.19	0.26	0.47	0.18	0.50	0.006	0.009	0.17	0.25	0.27	0.28
2.....	0.48	0.26	0.012	0.012	0.16	0.47	0.71	0.32	0.64	0.16	0.40	0.76	0.46	0.62	0.010	0.013	0.26	0.45	0.38	0.40
3.....	0.54	0.39	0.019	0.019	0.14	0.26	0.46	0.27	0.68	0.24	0.33	0.68	0.25	0.50	0.009	0.009	0.19	0.49	0.33	0.19
5.....	0.40	0.33	0.009	0.010	0.18	0.43	0.56	0.29	0.60	0.23	0.31	0.54	0.22	0.69	0.007	0.010	0.35	0.34	0.39	0.36
6.....	0.57	0.44	0.016	0.019	0.31	0.60	0.49	0.36	0.68	0.48	0.66	1.16	0.29	0.89	0.012	0.020	0.48	0.60	0.43	0.40
7.....	0.58	0.28	0.012	0.016	0.20	0.48	0.55	0.31	0.71	0.27	0.55	1.07	0.31	1.27	0.008	0.014	0.48	0.55	0.51	0.67
8.....	0.41	0.24	0.011	0.010	0.17	0.35	0.41	0.25	0.42	0.28	0.33	0.53	0.25	0.38	0.008	0.009	0.33	0.31	0.40	0.18
9.....	0.35	0.21	0.007	0.011	0.15	0.25	0.33	0.22	0.36	0.18	0.32	0.58	0.23	0.51	0.005	0.009	0.28	0.32	0.38	0.13
11.....	0.92	0.45	0.025	0.025	0.34	0.71	0.93	0.47	0.68	0.52	0.54	1.18	0.47	1.54	0.012	0.022	0.72	0.92	0.65	0.55
12.....	0.22	0.14	0.004	0.005	0.12	0.18	0.29	0.17	0.21	0.12	0.45	0.37	0.11	0.42	0.005	0.005	0.17	0.20	0.13	0.20
13.....	0.57	0.34	0.019	0.022	0.33	0.56	0.72	0.44	0.72	0.48	0.47	0.96	0.30	0.79	0.014	0.013	0.47	0.29	0.40	0.42
14.....	0.28	0.30	0.015	0.015	0.15	0.41	0.36	0.26	0.37	0.22	0.24	0.65	0.31	0.44	0.007	0.006	0.16	0.30	0.49	0.23
15.....	0.46	0.36	0.013	0.013	0.18	0.31	0.45	0.37	0.65	0.24	0.31	0.72	0.19	0.79	0.005	0.011	0.29	0.43	0.41	0.24
16.....	0.26	0.17	0.011	0.012	0.09	0.20	0.26	0.13	0.27	0.13	0.19	0.36	0.13	0.25	0.004	0.005	0.14	0.16	0.27	0.12
17.....	0.32	0.22	0.008	0.010	0.11	0.27	0.27	0.16	0.43	0.14	0.29	0.32	0.25	0.46	0.007	0.007	0.30	0.23	0.32	0.21
18.....	0.31	0.24	0.015	0.016	0.20	0.28	0.31	0.18	0.27	0.14	0.25	0.66	0.19	0.37	0.006	0.007	0.19	0.17	0.23	0.17
19.....	0.32	0.21	0.009	0.012	0.15	0.31	0.42	0.18	0.48	0.16	0.52	0.56	0.24	0.66	0.009	0.008	0.19	0.29	0.37	0.21
20.....	0.28	0.14	0.009	0.010	0.11	0.28	0.23	0.15	0.27	0.18	0.29	0.38	0.12	0.39	0.005	0.006	0.15	0.12	0.19	0.13
21.....	1.01	0.78	0.025	0.024	0.33	0.95	0.86	0.68	0.85	0.26	0.72	1.52	0.40	1.19	0.008	0.014	0.46	0.68	0.51	0.43
22.....	0.69	0.55	0.022	0.028	0.26	0.58	0.86	0.56	0.96	0.49	1.04	1.56	0.38	0.99	0.015	0.018	0.49	0.46	0.39	0.44
23.....	0.37	0.23	0.012	0.013	0.13	0.33	0.39	0.29	0.67	0.28	0.48	0.54	0.34	0.76	0.009	0.013	0.35	0.28	0.37	0.26

TABLE 4
CORRECTIONS TO THE LICK SYSTEM

Index	Offset (Lick/IDS−This Paper)
$H\delta_A$	0.01 ± 0.20 Å
$H\delta_F$	−0.07 ± 0.24 Å
CN_1	0.001 ± 0.007 mag
CN_2	0.008 ± 0.008 mag
Ca4227	0.13 ± 0.13 Å
G4300	−0.13 ± 0.21 Å
$H\gamma_A$	0.18 ± 0.23 Å
$H\gamma_F$	0.01 ± 0.04 Å
Fe4383	0.52 ± 0.35 Å
Ca4455	0.09 ± 0.26 Å
Fe4531	0.30 ± 0.24 Å
$C_2$4668	0.13 ± 0.18 Å
$H\beta$	−0.02 ± 0.02 Å
Fe5015	0.16 ± 0.42 Å
Mg_1	0.006 ± 0.006 mag
Mg_2	0.008 ± 0.005 mag
Mg *b*	0.08 ± 0.15 Å
Fe5270	0.11 ± 0.16 Å
Fe5335	0.06 ± 0.28 Å
Fe5406	0.03 ± 0.15 Å

diagnostic indices are luminosity-weighted. Thus, the interpretation of the Hβ 7 Gyr age estimate could either be taken at face value or reflect a very small amount (in terms of the mass involved) of recent star formation, superposed on an underlying ancient stellar population that entirely dominates the mass fraction. To quantify the latter possibility, we first note that the Hβ value (at fixed metallicity) of a 13 Gyr TMK04 stellar population is ∼1.37, implying a difference of ∼0.18 in index strength between 7 and 13 Gyr. Using Worthey (1994) models at solar metallicity, only 4% of 2 Gyr light (or 1% of 1 Gyr light) mixed with a 13 Gyr underlying population would be needed to produce the observed effect.

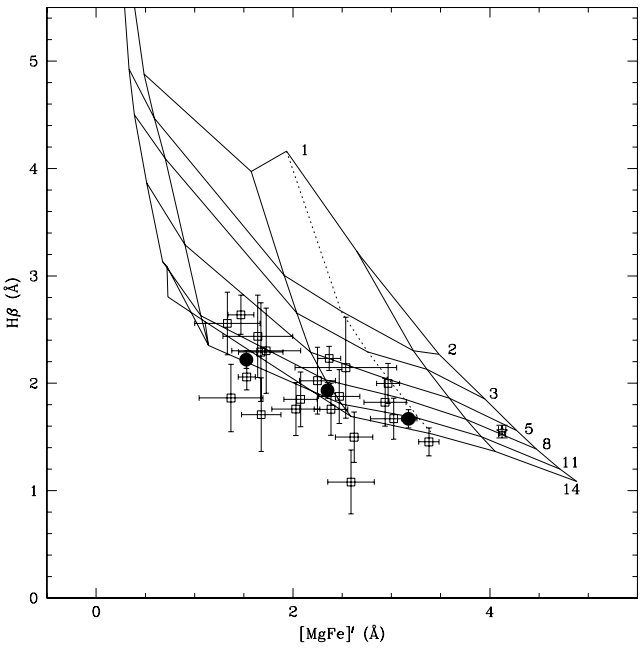

FIG. 3.—Hβ-[MgFe]′ diagnostic diagram for the GCs (*squares*) and central $r_e/8$ integrated light (*star*) of the elliptical galaxy NGC 4365. The circles represent weighted means for the three subpopulations (see text). Overlain are SSP model grids from TMK04. The isochrone ages are 1, 2, 3, 5, 8, 11, and 14 Gyr (*top to bottom*). The isosiders (constant-metallicity lines) are [Z/H] = −2.25, −1.33, −0.33, 0 (*dotted line*), 0.33, and 0.67 (*left to right*). All the clusters appear to be old.

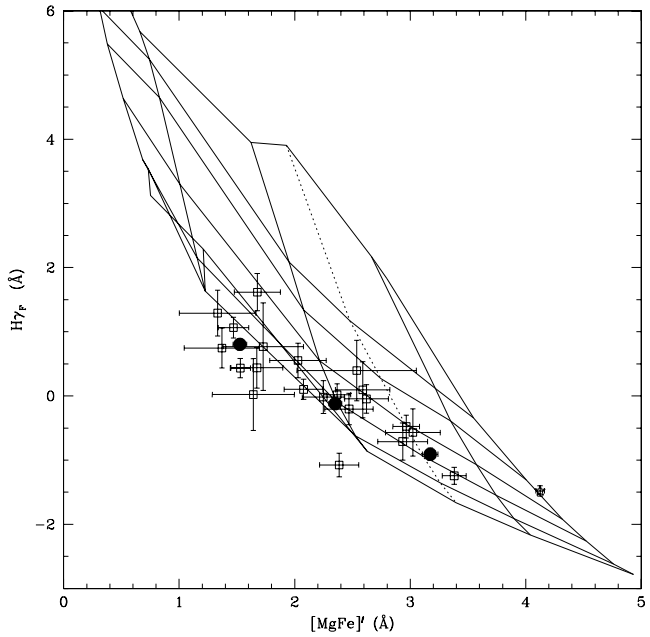

FIG. 4.—Hγ_F-[MgFe]′ diagram. Symbols and grid identities are the same as in Fig. 3.

3.3. *Comparison to Previous Work*

In Paper I the measured spectral indices showed substantial scatter along the locus of the age-metallicity degeneracy. The indices of some GCs (particularly Hβ) fell below the SSP grid, formally suggesting very old ages. This is a well-known problem with GC indices (e.g., Proctor et al. 2004). At the other extreme, some GCs occupied the intermediate-age, high-metallicity region of the model grid, exactly as expected from the photometric

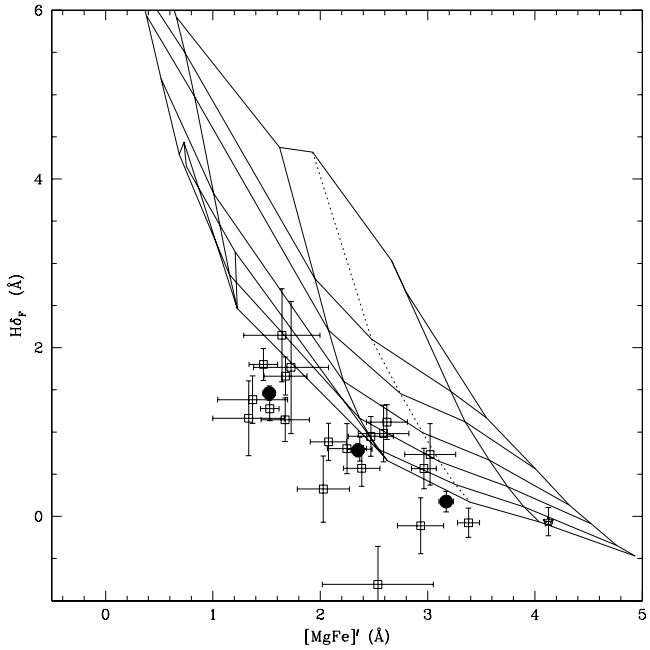

FIG. 5.—Hδ_F-[MgFe]′ diagram. Symbols and grid identities are the same as in Fig. 3. Three old subpopulations of GCs are apparent.

TABLE 5
Spectroscopic Metallicity Estimates and Subpopulations

ID	PCA [m/H] (dex)	χ^2 [m/H] (dex)	Subpopulation
1.....	−1.10	−1.08	Blue
2.....	−1.01	−0.95	Blue
3.....	−0.61	−0.68	Orange
5.....	−0.12	−0.23	Red
6.....	−1.34	−1.18	Blue
7.....	−1.13	−1.03	Blue
8.....	−0.36	−0.28	Orange
9.....	−0.32	−0.53	Orange
11.....	−0.43	−0.23	Orange
12.....	−0.52	−0.40	Orange
13.....	−0.25	−0.25	Orange
14.....	−0.46	−0.43	Orange
15.....	−0.21	−0.18	Red
16.....	0.18	0.03	Red
17.....	−0.60	−0.48	Orange
18.....	−0.20	−0.13	Red
19.....	−0.49	−0.43	Orange
20.....	−0.90	−0.85	Blue
21.....	−0.73	−0.85	Blue
22.....	−1.01	−0.85	Blue
23.....	−1.04	−1.08	Blue

work of Puzia et al. (2002). However, it appears that this was largely due to relatively low S/N spectra (more than 50% lower than the present work), with errors causing GCs to spread out along the age-metallicity locus. Some lower S/N spectra appear to have been affected by sky subtraction difficulties because of superposition on the bright, strongly spatially varying galaxy background. Independent, careful re-reductions of the original data set gave index values consistent within the errors with those published in Paper I. However, some of these index values differ significantly (by 1 Å or more) from the indices measured on the three overlapping objects in this paper, indicating systematic uncertainties in addition to the formal (photon-statistical) errors. These results reinforce the need for high S/N data, at as high a resolution as possible, for studies of extragalactic GCs.

3.4. *Metallicities*

We derived metallicities for our sample clusters using principal component analysis (PCA)–based metallicities (Strader & Brodie 2004) for a subset of 11 Lick indices, as well as the Proctor et al. (2004) χ^2 minimization technique. These values can be found in Table 5. The typical formal error on these PCA metallicities is 0.1 dex, but the systematic error may be 0.1–0.2 dex or even larger if the cluster is not in the metallicity range $-1.7 < [\mathrm{m/H}] < 0$ (see Strader & Brodie 2004 for more details). Typical χ^2 [m/H] errors are 0.2–0.3 dex. The mean [m/H] and σ values of each of the three subpopulations for the PCA and χ^2 methods are -1.02 ± 0.17 and -0.98 ± 0.13 (blue); -0.45 ± 0.12 and -0.41 ± 0.14 (orange); and -0.09 ± 0.18 and -0.13 ± 0.11 (red). These mean metallicities are consistent, both with each other and with the values qualitatively apparent in Figures 3–5.

3.5. *Abundance Ratios*

In Figure 6 we compare our measurements of Mg *b* against ⟨Fe⟩ with 3 and 14 Gyr model isochrones from TMK04. The intermediate-metallicity and metal-rich GCs in our sample have [α/Fe] around +0.3 or higher. The metal-poor GCs have slightly lower [α/Fe] at ∼+0.2. Anomalously low abundance ratios (solar or lower) have been seen in metal-poor GCs in the elliptical NGC 3610 (Strader et al. 2004) and in several spirals in the Sculptor Group (Olsen et al. 2004); these studies also used the TMK04 models. This may suggest a systematic problem with these models at low metallicities.

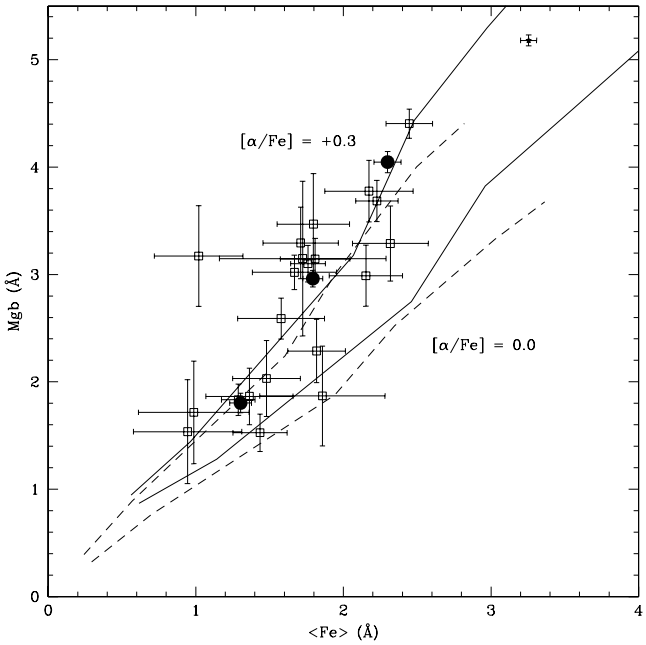

Fig. 6.—Mg*b*-⟨Fe⟩ diagram. Symbols are the same as in Fig. 3. Shown are 14 Gyr (*solid lines*) and 3 Gyr (*dashed lines*) isochrones for the labeled [α/Fe] ratios (from TMK04). The GCs are α-enhanced to values typical of Galactic GCs.

Figure 7 shows that the Lick CN_2 values of the NGC 4365 GCs are comparable to those of Galactic GCs of similar metallicity

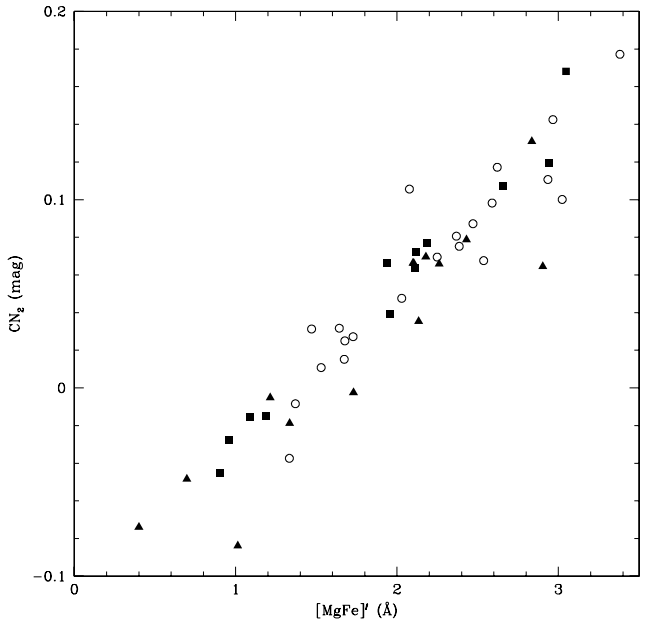

Fig. 7.—CN_2-[MgFe]′ diagram. Plotted are our sample GCs (*circles*) and Galactic GCs from Puzia et al. (2002) and Gregg (1994) (*squares and triangles, respectively*). The NGC 4365 GCs do not appear to be enhanced in CN with respect to Galactic GCs; however, the sensitivity of CN_2 to CN variations is weak (see text).

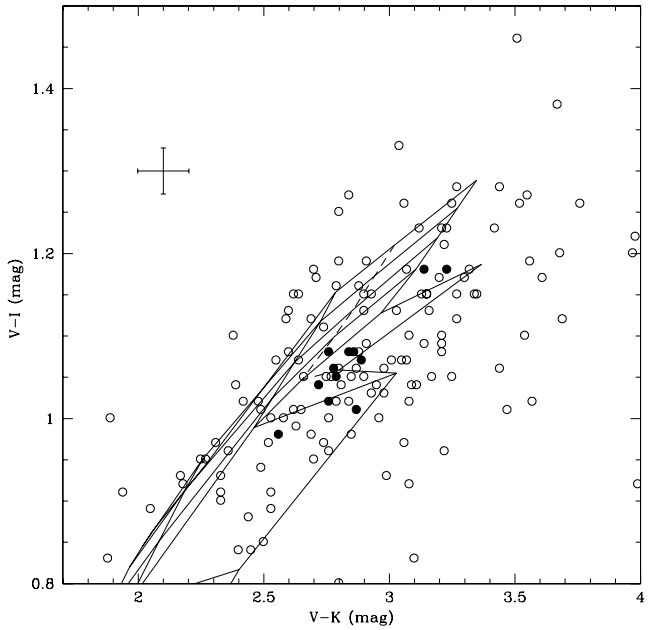

FIG. 8.—$V-K$ vs. $V-I$ color-color diagram for NGC 4365 GCs (*circles*). Filled circles represent GCs with spectroscopic data, either from this work or Paper I. Note our successful sampling of the region with candidate intermediate-age clusters. The median photometric error is shown. The overplotted model grid is from Maraston (2005). The isochrone ages are 2, 3, 5, 8, 11, and 14 Gyr (*bottom to top*). The isosiders (constant-metallicity lines) are $[Z/H] = -1.33$, -0.33, 0 (*dashed line*), and 0.33 (*left to right*).

(which, in turn, are enhanced with respect to local subdwarfs). However, the CN_2 index measures the $\Delta v = -1$ 4215 Å band, which is rather weak compared to the $\Delta v = 0$ 3883 Å band. Indeed, M31 GCs are clearly enhanced in the UV band (attributed primarily to nitrogen; Brodie & Huchra 1991; Worthey 1998) but are quite similar to Galactic GCs in their CN_2 indices (Beasley et al. 2004), indicating the low sensitivity of the Lick index to CN variations. At present, the typical CN enhancement for GCs is unclear.

4. PHOTOMETRY

Figure 8 is a $V-I$ versus $V-K$ plot for GC candidates in NGC 4365 along with SSP model grids from Maraston (2005). GCs with Keck spectroscopy (both from this work and from Paper I) are indicated by filled circles. The *VIK* data are from Puzia et al. (2002), who suggested that the distribution of GCs in this color-color diagram reflected the presence of an intermediate-age (ranging from 2 to 5 Gyr) subpopulation with solar to super-solar metallicities. Clearly, the spectroscopically observed GCs nicely sample the region in which the intermediate-age GCs would be expected to lie.

Assuming that the higher S/N spectroscopic data and the improvements in the SSP models correctly reflect old ages for the entire GC sample, we might conclude that the spectroscopic and photometric data are not entirely consistent. Figure 9 illustrates this point. The $V-I$ versus $V-K$ color distribution of the NGC 4365 GC system (Fig. 9, *left*) is compared to that of NGC 3115 (Fig. 9, *right*), an S0 galaxy with a "normal" GC color distribution, displaying the bimodality in $V-I$ typical of luminous galaxies. Spectroscopy of NGC 3115 GCs shows that both the blue and the red GCs are coeval and old (Kuntschner

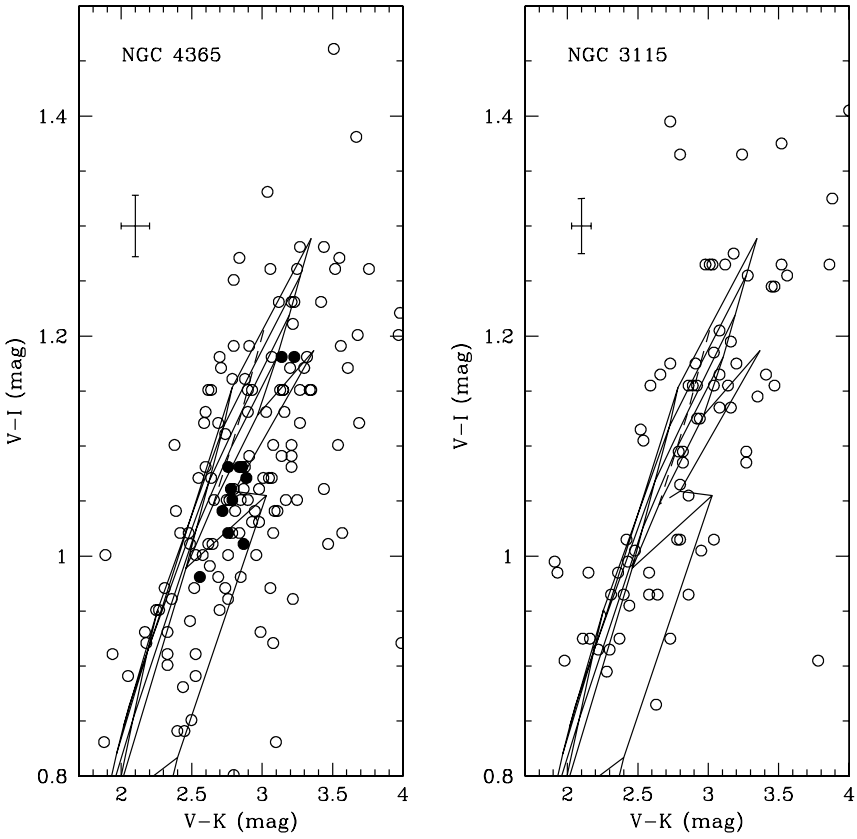

FIG. 9.—$V-K$ vs. $V-I$ color-color diagrams for GCs in NGC 4365 and NGC 3115. The left panel is identical to Fig. 8. The right panel clearly shows the two normal GC subpopulations, which are not apparent in the NGC 4365 panel. Median photometric errors are shown. The model grids are from Maraston (2005), and grid identities are the same as in Fig. 8.

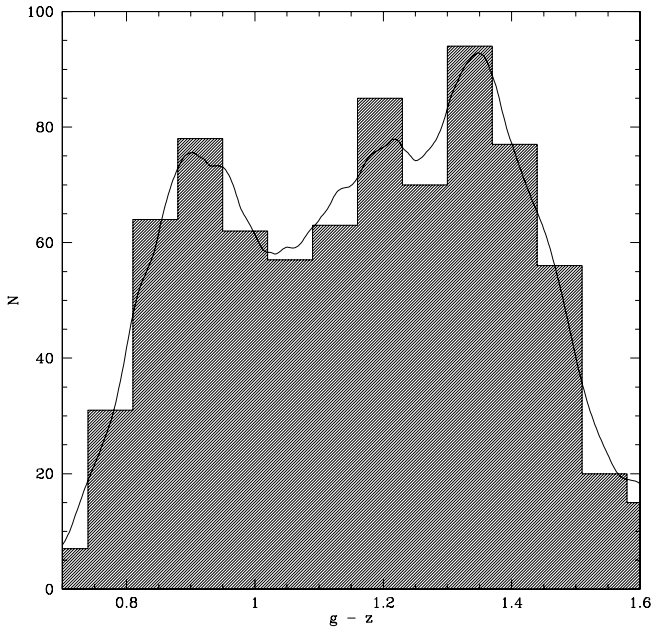

FIG. 10.—*HST* ACS $g - z$ color histogram for NGC 4365 clusters. The solid line indicates a density estimate using an Epanechikov kernel. The histogram appears trimodal, with peaks at ~0.90, 1.22, and 1.34.

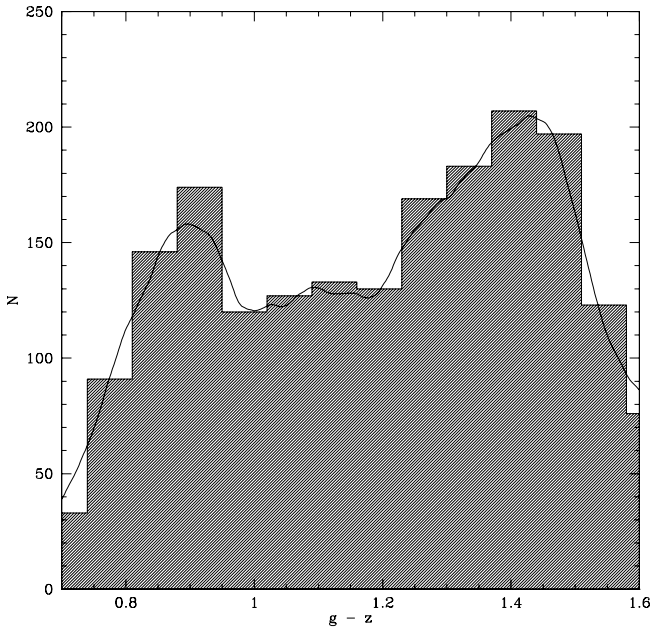

FIG. 11.—*HST* ACS $g - z$ color histogram for M87 clusters. The solid line indicates a density estimate using an Epanechikov kernel. The two normal subpopulations are apparent at ~0.89 and 1.42.

et al. 2002). However, if all the NGC 4365 GCs are old as well, why do the color distributions of these two galaxies look so different?

To try to address this question we have performed photometry for the central portion of the GC system using archival g and z *HST* ACS images obtained as part of the ACS Virgo Cluster Survey (Côté et al. 2004). Frames were processed through the standard pipeline, including *multidrizzle* for image combining and rejection of cosmic rays. GC candidates were detected on 20×20 pixel median-subtracted images. We performed photometry through a 5 pixel (0.″25) radius aperture and corrected to a 10 pixel aperture using corrections derived from bright objects of a range of sizes. These 10 pixel magnitudes were then corrected to a nominal infinite aperture using the values in M. Sirianni et al. (2005, in preparation). These g and z magnitudes are on the AB system, using the zero points in Jordán et al. (2004). All photometry has been corrected for reddening using the maps of Schlegel et al. (1998). The resulting color histogram is shown in Figure 10, and in Figure 11 we show a similar histogram constructed for M87. In both histograms, density estimates using an Epanechikov kernel with a small bin size are overplotted. The apparent interpretation of the NGC 4365 histogram is that the GC colors are trimodal in $g - z$, with peaks at ~0.90, 1.22, and 1.34 (with errors $\sim \pm 0.02$–0.03), although it was found to be unimodal in $V - I$. However, the significance of the three peaks cannot be readily assessed. Experimentation with Kaye's mixture model (KMM) tests (Ashman et al. 1994) on simulated color distributions gave falsely high levels of significance for subpopulations that were not actually present, suggesting that this technique cannot be reliably applied to this multimodal data. We note that there have been previous claims in the literature for trimodal GC subpopulations (e.g., Ostrov et al. 1993), but to our knowledge NGC 4365 is the first galaxy with supporting spectroscopic evidence.

To determine whether any of these three observed peaks are consistent with values expected from the galaxy luminosity–GC color relation for the blue or red subpopulations (Forbes et al. 1997; Larsen et al. 2001; Strader et al. 2004), a conversion between $V - I$ and $g - z$ is required. A rough conversion may be made with reference to M87, which has been observed in both colors. In M87 the $V - I$ peaks are at 0.96 and 1.18, while the $g - z$ peaks are at 0.89 and 1.42. Thus, a crude preliminary conversion equation is $V - I = 0.42(g - z) + 0.59$. Note that this equation assumes no age difference between the two populations; this is consistent with our spectroscopic results. A corresponding linear fit to Maraston (2005) SSP models for broadband colors (using model parameters of 13 Gyr and a Kroupa initial mass function) gives a similar relation with a slightly steeper slope: $V - I = 0.49(g - z) + 0.45$. Our empirical formula suggests that the blue and red peaks in NGC 4365 occur at $V - I \sim$ 0.96 and 1.15, respectively. The values predicted by the galaxy luminosity–GC color relations are 0.93 and 1.17, implying that these converted $g - z$ blue and red peaks do indeed place NGC 4365 approximately on the normal relation. A plausible explanation is that the intermediate-metallicity peak filled in the gap between the two regular subpopulations in the original $V - I$ data, resulting in an abnormally broad, apparently unimodal distribution. A more detailed analysis of the consistency of ACS and WFPC2 photometry, as well as new New Technology Telescope SOFI K photometry for NGC 4365 GCs, is forthcoming in S. S. Larsen et al. (2005, in preparation).

Eleven of the 21 GCs in our sample fall within the field of view of the ACS imaging and thus have $g - z$ colors. To test whether the trimodality observed in the $g - z$ color histogram is the same as that seen in the Lick index-index plots, we calculated the mean color for each of the spectroscopic groups. Of the 11 spectroscopically observed GCs with ACS colors, two are blue, six are orange, and three are red. The corresponding mean colors are $g - z = 0.96$, 1.21, and 1.32—quite similar to the peaks in the color histogram, especially when the small sample size is considered. Both the spectroscopy and the *HST* optical photometry point to a consistent picture of three old subpopulations of GCs in NGC 4365. However, spectroscopy of a larger sample of GCs would be useful to test this conclusion.

Finally, we note that within the ACS field of view, the orange GCs appear to be very centrally concentrated, with few located

outside a radius of $\sim 1'$. By contrast, the red and blue GCs extend to the edges of the ACS images. As is typical in massive galaxies, the blues are less concentrated than the reds (Larsen et al. 2001).

5. DISCUSSION AND CONCLUSIONS

If these results are confirmed, NGC 4365 would be the first galaxy found to contain three old subpopulations of GCs. Is this elliptical galaxy a pathological anomaly or simply in the tail of a distribution of multimodal GC systems waiting to be discovered? Models that consider the formation of GCs in the hierarchical merging paradigm of galaxy formation (e.g., Beasley et al. 2002) naturally predict substructure as a straightforward consequence of the complex merging histories of massive early-type galaxies. While Beasley et al. (as well as the bulk of other semianalytic models from several years ago) predict significant *age* substructure in the star formation histories of these galaxies, more recent *N*-body/hydrodynamic models suggest early, rapid formation (e.g., Nagamine et al. 2004). This is consistent with the old ages of all three GC subpopulations in NGC 4365. However, there remains the question of why this galaxy has three rather than two clear subpopulations.

As mentioned above, the galaxy does not have properties notably different from those of other elliptical galaxies of similar luminosity and environment. The main body and counter-rotating core of the galaxy both appear to be old and α-enhanced (Davies et al. 2001), although this depends on the SSP model used (see above). The $L_{B_\odot}/L_X$ ratio is typical for a galaxy of its luminosity (O'Sullivan et al. 2001). Its strong triaxiality precludes the presence of a central black hole significantly more massive than that predicted by the M-σ relation (Statler et al. 2004). In short, the GC system of this galaxy is the most abnormal thing about it.

The fact that the metal-poor and metal-rich GC peaks lie at the values predicted for a galaxy of this luminosity suggests that the intermediate-metallicity peak is the "interloper" in an otherwise normal GC system. The observed colors of this orange subpopulation ($g - z = 1.22 \sim V - I = 1.10$) correspond to galaxies with $M_V \sim -17$ in the red GC relation of Larsen et al. (2001). Galaxies of this luminosity have very few GCs, and it is not yet clear whether, in general, they have a red peak at all (Lotz et al. 2004). Indeed, the typical size of the *entire* GC system of a single $M_V = -17$ galaxy is $\sim$20–30 GCs, compared with hundreds or more orange GCs in NGC 4365. Thus, accretion (Côté et al. 2002) is an unlikely explanation for this extra subpopulation.

The large number of these intermediate-metallicity clusters implies an unusual, quite important star formation event early in the history of the galaxy that might also have formed a significant fraction of the field star population. To estimate the amount of gas involved in such an event, we adopt a typical GC formation efficiency of 0.25% (McLaughlin 1999) and a typical GC mass of $3 \times 10^5\ M_\odot$. Roughly $1.2 \times 10^8\ M_\odot$ of gas is needed to form one new GC (Harris 2003). A galaxy of the luminosity of NGC 4365 typically has similar numbers of metal-poor and metal-rich GCs (Forbes & Forte 2001); our color histogram suggests that perhaps 40% of the nonblue GCs (thus, $\sim$20% of the total GC population) are of intermediate metallicity. For a total GC population of $\sim$2500 (Ashman & Zepf 1998), this would imply that $\sim$500 orange clusters are formed. The corresponding gas mass is large, $6 \times 10^{10}\ M_\odot$.

However, if the field stars are primarily old, the intermediate-metallicity population would probably not be noticeable in the integrated spectrum of the galaxy itself. The luminosity-weighted metallicity of the galaxy would appear slightly lower than otherwise but far less than would be needed to make the galaxy an outlier in the metallicity hyperplane (Trager et al. 2000). A color-magnitude diagram of the red giant branch of the galaxy itself (possible with a 30 m telescope) will probably be needed to quantitatively understand the relative importance of this star formation event in building up the galaxy's stellar mass.

In conclusion, we find evidence of three old subpopulations of GCs in NGC 4365. No metal-rich intermediate-age GCs are apparent, although the size (21 GCs) and spatial distribution (few within the central 4 kpc) of our sample are caveats to our results. The highly multiplexing spectrographs now on 8–10 m class telescopes (e.g., Keck DEIMOS and VLT VIMOS) could permit one to obtain spectra of 100–150 GCs in a single slit mask. However, the strong central concentration of GC systems (with typical surface densities of $\sim r^{-1.5}$ to r^{-2}) will likely limit such studies to the most populous systems for the foreseeable future.

Our results also indicate that it is difficult to identify intermediate-age GCs solely from broadband photometry, even if a near-infrared band is used. It will be interesting to see if evidence of significant intermediate-age subpopulations in other galaxies, e.g., NGC 5846 (Hempel et al. 2003), is supported by spectroscopic follow-up.

We thank the anonymous referee for detailed comments on this paper. We are grateful to Thomas Puzia for providing us with his photometry and to Claudia Maraston and Daniel Thomas for early access to their models, as well as helpful discussions. Ricardo Schiavon provided useful insights. This work was supported by NSF grant AST 02-06139. J. S. acknowledges support from an NSF Graduate Research Fellowship. A. J. C. acknowledges financial support from a UCM Fundación del Amo Fellowship. Spectroscopic data presented herein were obtained at the W. M. Keck Observatory, which is operated as a scientific partnership among the California Institute of Technology, the University of California, and the National Aeronautics and Space Administration. The Observatory was made possible by the generous financial support of the W. M. Keck Foundation. The authors wish to recognize and acknowledge the very significant cultural role and reverence that the summit of Mauna Kea has always had within the indigenous Hawaiian community. We are most fortunate to have the opportunity to conduct observations from this mountain.

REFERENCES

Ashman, K., Bird, C. M., & Zepf, S. E. 1994, AJ, 108, 2348
———. 1998, Globular Cluster Systems (Cambridge: Cambridge Univ. Press)
Beasley, M. A., Baugh, C. M., Forbes, D. A., Sharples, R. M., & Frenk, C. S. 2002, MNRAS, 333, 383
Beasley, M. A., Brodie, J. P., Strader, J., Forbes, D. A., Proctor, R. N., Barmby, P., & Huchra, J. P. 2004, AJ, 128, 1623
Brodie, J. P., & Huchra, J. P. 1991, ApJ, 379, 157
Côté, P., West, M. J., & Marzke, R. O. 2002, ApJ, 567, 853
Côté, P., et al. 2004, ApJS, 153, 223
Davies, R. L., et al. 2001, ApJ, 548, L33
Denicoló, G., Terlevich, R., Terlevich, E., Forbes, D. A., Terlevich, A., & Carrasco, L. 2005, MNRAS, 356, 1440
de Vaucouleurs, G., de Vaucouleurs, A., Corwin, H. G., Jr., Buta, R. J., Paturel, G., & Fouque, P. 1991, Third Reference Catalogue of Bright Galaxies (New York: Springer)
Forbes, D. A. 1996, AJ, 112, 954
Forbes, D. A., Brodie, J. P., & Grillmair, C. J. 1997, AJ, 113, 1652
Forbes, D. A., & Forte, J. C. 2001, MNRAS, 322, 257

Gebhardt, K., & Kissler-Patig, M. 1999, AJ, 118, 1526
Gregg, M. D. 1994, AJ, 108, 2164
Harris, W. E. 2003, in Extragalactic Globular Cluster Systems, ed. M. Kissler-Patig (Berlin: Springer), 317
Hempel, M., Hilker, M., Kissler-Patig, M., Puzia, T. H., Minniti, D., & Goudfrooij, P. 2003, A&A, 405, 487
Jordán, A., et al. 2004, ApJS, 154, 509
Kundu, A., & Whitmore, B. C. 2001, AJ, 121, 2950
Kuntschner, H., Ziegler, B. L., Sharples, R. M., Worthey, G., & Fricke, K. J. 2002, A&A, 395, 761
Larsen, S. S., Brodie, J. P., Beasley, M. A., Forbes, D. A., Kissler-Patig, M., Kuntschner, H., & Puzia, T. H. 2003, ApJ, 585, 767 (Paper I)
Larsen, S. S., Brodie, J. P., Huchra, J. P., Forbes, D. A., & Grillmair, C. 2001, AJ, 121, 2974
Lotz, J. M., Miller, B. W., & Ferguson, H. C. 2004, ApJ, 613, 262
Maraston, C. 2005, MNRAS, submitted
Maraston, C., Kissler-Patig, M., Brodie, J. P., Barmby, P., & Huchra, J. P. 2001, A&A, 370, 176
McLaughlin, D. E. 1999, AJ, 117, 2398
Nagamine, K., Cen, R., Hernquist, L., Ostriker, J. P., & Springel, V. 2004, ApJ, 610, 45
Oke, J., et al. 1995, PASP, 107, 375
Olsen, K. A. G., Miller, B. W., Suntzeff, N. B., Schommer, R. A., & Bright, J. 2004, AJ, 127, 2674
Ostrov, P., Geisler, D., & Forte, J. C. 1993, AJ, 105, 1762
O'Sullivan, E., Forbes, D. A., & Ponman, T. J. 2001, MNRAS, 328, 461
Proctor, R. N., Forbes, D. A., & Beasley, M. A. 2004, MNRAS, 355, 1327
Puzia, T. H., Zepf, S. E., Kissler-Patig, M., Hilker, M., Minniti, D., & Goudfrooij, P. 2002, A&A, 391, 453
Schiavon, R. P., Rose, J. A., Courteau, S., & MacArthur, L. A. 2004, ApJ, 608, L33
Schlegel, D. J., Finkbeiner, D. P., & Davis, M. 1998, ApJ, 500, 525
Statler, T. S., Emsellem, E., Peletier, R. F., & Bacon, R. 2004, MNRAS, 353, 1
Strader, J., & Brodie, J. P. 2004, AJ, 128, 1671
Strader, J., Brodie, J. P., & Forbes, D. A. 2004, AJ, 127, 3431
Surma, P., & Bender, R. 1995, A&A, 298, 405
Thomas, D., Maraston, C., & Bender, R. 2003, MNRAS, 339, 897 (TMB03)
Thomas, D., Maraston, C., & Korn, A. 2004, MNRAS, 351, L19 (TMK04)
Trager, S. C., Faber, S. M., Worthey, G., & González, J. J. 2000, AJ, 120, 165
Trager, S. C., Worthey, G., Faber, S. M., Burstein, D., & Gonzalez, J. J. 1998, ApJS, 116, 1
Vazdekis, A. 1999, ApJ, 513, 224
Worthey, G. 1994, ApJS, 95, 107
———. 1998, PASP, 110, 888
Worthey, G., Faber, S., González, J., & Burstein, D. 1994, ApJS, 94, 687
Worthey, G., & Ottaviani, D. L. 1997, ApJS, 111, 377